

Article

A Near-Hover Adaptive Attitude Control Strategy of a Ducted Fan Micro Aerial Vehicle with Actuator Dynamics

Shouzhao Sheng * and Chenwu Sun

College of Automation Engineering, Nanjing University of Aeronautics and Astronautics, 29 YuDao Street, Nanjing 210016, China; E-Mail: sunchenwu@nuaa.edu.cn

* Author to whom correspondence should be addressed; E-Mail: shengsz@nuaa.edu.cn; Tel.: +86-25-8489-2305; Fax: +86-25-8489-2301.

Academic Editor: Dimitrios G. Aggelis

Received: 11 August 2015 / Accepted: 23 September 2015 / Published: 28 September 2015

Abstract: The aerodynamic parameters of ducted fan micro aerial vehicles (MAVs) are difficult and expensive to precisely measure and are, therefore, not available in most cases. Furthermore, the actuator dynamics with risks of potentially destabilizing the overall system are important but often neglected consideration factors in the control system design of ducted fan MAVs. This paper presents a near-hover adaptive attitude control strategy of a prototype ducted fan MAV with actuator dynamics and without any prior information about the behavior of the MAV. The proposed strategy consists of an online parameter estimation algorithm and an adaptive gain scheduling algorithm, with the former accommodating parametric uncertainties, and the latter approximately eliminating the coupling among axes and guaranteeing the control quality of the MAV. The effectiveness of the proposed strategy is verified numerically and experimentally.

Keywords: parameter estimation; adaptive gain scheduling; attitude control; ducted fan micro aerial vehicle

1. Introduction

The ducted fan micro aerial vehicle (MAV) with small size and compact structure is used mainly for low-speed flight missions in addition to hover, vertical takeoff, and landing capabilities. Compared to a conventional configuration micro unmanned helicopter (MUH) or a multi-rotor craft (MRC), the ducted fan MAV is a much safer platform since its propeller is mounted inside the duct which can act as a shield

to avoid the risk of injury. The MUH and MRC, however, are rather dangerous due to the exposed rotor blades.

Although many related research was previously almost under stagnation, ducted fan MAVs have recently attracted great interest, such as Cypher [1], iSTAR9 [2], and HoverEye [3]. Again, the studies have been conducted for ducted fan MAVs, mainly including multidisciplinary design optimization [4,5], system modeling [6–8], and control design [9–12]. As for the control design, Pflimlin systematically developed the aerodynamic model and the attitude and position control systems for a ducted fan MAV with considering the crosswind, gyroscopic coupling and unknown aerodynamics, and successfully demonstrated the proposed control strategies on the HoverEye platform [13,14]. The results of these investigations have certainly shown that the proposed control strategies, mainly based on decoupling and backstepping techniques, can significantly enhance the flight performance of the MAV with guaranteed stability. Sliding mode techniques are developed for improving the control qualities of ducted fan MAVs in [15,16], which show superior performance over classical control techniques when variations in vehicle dynamics and actuator characteristics are introduced. Spaulding [17] adopted a nonlinear dynamic inversion method, and Chwa [18] proposed a compensator to accommodate for the effect of the actuator dynamics. However, most of these methods heavily rely on accurate dynamic models that are difficult to obtain, and the resulting performance is deteriorated in practical applications, especially in the presence of measurement noises. Other existing methods include PID control [19], linear-quadratic regulator (LQR) [20], robust control [21,22], neural adaptive control [23], fuzzy control [24,25], and nonlinear feedback control [26], *etc.* The actuator dynamics, however, have not been systematically considered, derived, and applied in the control system design.

Overall, most related studies reported in the literature are based on the assumption that the actuator dynamics are fast enough to be negligible. However, the actuators actually show limited performance in real situations and, accordingly, the control qualities would be severely degraded if the actuator dynamics are neglected.

In this study, a near-hover adaptive attitude control strategy is designed for a prototype ducted fan MAV. The combination of online parameter estimation and adaptive gain scheduling algorithms in the proposed strategy can accommodate parametric uncertainties and approximately eliminate the coupling among axes, which can simultaneously lead to enhance the resulting performance. The proposed strategy is tested and the results also illustrate that it can significantly improve the flight performance of the MAV.

This paper is organized as follows: Section 2 is devoted to the description of the attitude control problem of the prototype ducted fan MAV. The adaptive attitude control strategy of the MAV with actuator dynamics is formulated in Section 3, and experimental tests are presented in Section 4. The last section offers conclusions.

2. The Attitude Control Problem Statement of the Prototype Ducted Fan MAV

The prototype small-size ducted fan VTOL MAV, 0.8 m in height and 0.55 m in diameter, is shown in Figure 1. A duct is formed through the fuselage, and a ducted fan is mounted to the middle portion of the fuselage. Four deflecting vanes are mounted along the longitudinal and lateral axes of symmetry below the fan to provide pitch, roll, and yaw movements. Most of the anti-torque generated by the ducted

fan is compensated by the stators configured inside the duct while the remaining anti-torque is balanced by the deflecting vanes. A cent-symmetric landing gear consisting of four legs, *i.e.*, left, right, front, back, made from glass fiber reinforced plastics is installed on the MAV.

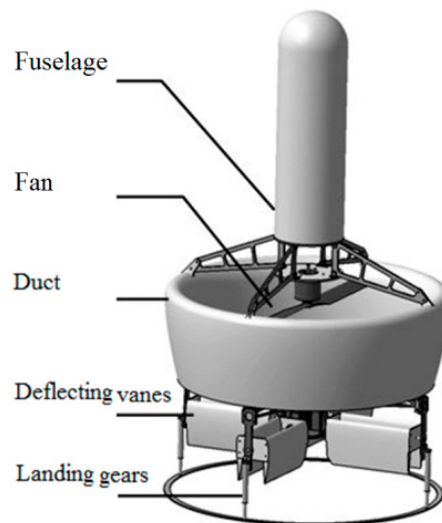


Figure 1. The prototype ducted fan MAV.

Ducted fan aerodynamics has been discussed in more detail in listed references. A total of four servo motors are installed on the fuselage. The movements of the servo motors can change the direction of deflecting vanes, enabling the MAV to fly in all directions (forward, backward, left, right, *etc.*). The movements of the left and right servo motors in the same directions can achieve pitch movement, while the movements of the front and back servo motors can achieve the roll movement. The movements of the opposite servo motors in the opposite direction can compensate the remaining anti-torque and further achieve yaw movement. Mathematically, the control allocation strategy is represented as:

$$\begin{bmatrix} \widehat{\delta}_l \\ \widehat{\delta}_r \\ \widehat{\delta}_f \\ \widehat{\delta}_b \end{bmatrix} = \begin{bmatrix} \frac{\widehat{\delta}_{pit}}{2} + \frac{\widehat{\delta}_{yaw}}{4} \\ \frac{\widehat{\delta}_{pit}}{2} - \frac{\widehat{\delta}_{yaw}}{4} \\ -\frac{\widehat{\delta}_{rol}}{2} + \frac{\widehat{\delta}_{yaw}}{4} \\ -\frac{\widehat{\delta}_{rol}}{2} - \frac{\widehat{\delta}_{yaw}}{4} \end{bmatrix} \quad (1)$$

The rotational speed of the ducted fan is maneuvered by one other servo motor to provide sufficient thrust force to lift the MAV. There is a sensor unit installed on the MAV to provide the flight controller with feedback signals containing measurement noises that increase the chatter in the input signal of actuators through feedback paths.

We assume that the fuselage is a rigid body. The nonlinear kinematic equations can then be defined as follows:

$$\dot{\widehat{X}} = f(\widehat{X}, \widehat{U}, \Theta) \quad (2)$$

where $\hat{X} = [\hat{u}, \hat{v}, \hat{w}, \hat{\theta}, \hat{\phi}, \hat{\psi}, \hat{q}, \hat{p}, \hat{r}]^T$ and $\hat{U} = [\hat{\delta}_{pit}, \hat{\delta}_{rol}, \hat{\delta}_{yaw}, \hat{\delta}_{rot}]^T$; Θ represents the aerodynamic parameter set, which is not available in most cases.

The nonlinear system can be linearized near the hover flight condition and the linearized model is given by:

$$\dot{X} = AX + BU \tag{3}$$

where $X = \hat{X} - X_e = [u, v, w, \theta, \phi, \psi, q, p, r]^T$ and $U = \hat{U} - U_e = [\delta_{pit}, \delta_{rol}, \delta_{yaw}, \delta_{rot}]^T$. X_e and U_e are the trim state and input vectors, respectively. However the determination of the trim condition is quite complicated due to the uncertainties in Θ . Therefore, the estimates of X_e and U_e are, respectively, denoted by:

$$X_0 = X_e + \tilde{X}, U_0 = U_e + \tilde{U} \tag{4}$$

Equation (3) should be rewritten as:

$$\dot{X} = AX + BU + E \tag{5}$$

where $X = \hat{X} - X_0, U = \hat{U} - U_0$ and $E = A\tilde{X} + B\tilde{U}$. Note that A, B and E are also unknown.

The MAV is used mainly for low-speed flight missions. However, unique pendulum-like motions of the MAV naturally arise from the unique symmetrical structure. The underdamped oscillatory modes consist of pitching and rolling moving oscillations with negligible vertical motion. The phenomenon of low amplitude self-sustained pitching and horizontal moving oscillations, for example, is more likely to occur in hover mode, as shown in Figure 2. Alternating flight speed u increases from zero at time t_0 to a maximum value at time t_1 in one direction, and decreases back to zero at time t_2 ; it then increases to a maximum value at time t_3 in the opposite direction and again decreases to zero at time t_4 . Alternating pitch angle θ changes in a similar manner, but there is a 90° phase difference between alternating pitch angle and alternating flight speed.

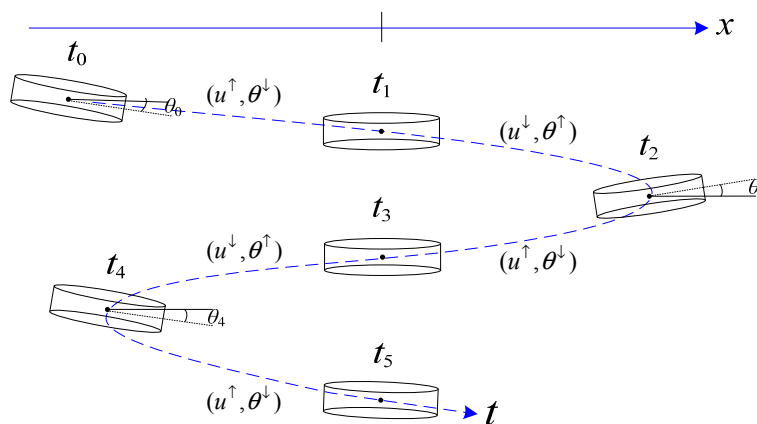


Figure 2. A schematic diagram illustrating the pitching and horizontal moving oscillations.

The development of a near-hover flight control system for the prototype MAV to avoid pendulum-like motions and endow it with good flying qualities is still a challenge since the dynamics are fully coupled and subject to parametric uncertainties. In addition, the actuator dynamics also add complexity to the development.

3. The Adaptive Attitude Control Strategy of the MAV with Actuator Dynamics

As the MAV is axis-symmetric, the pitch and the roll dynamics have a similar property. For this reason, this study is focused on the adaptive attitude control strategy of the pitch axis. Without loss of generality, the strategy can also apply to other axes.

3.1. The Online Parameter Estimation Method for the MAV

Referring to Equation (5), the linearized model of the pitch axis is given by:

$$\dot{q} = M_u^{\dot{q}}u + M_v^{\dot{q}}v + M_w^{\dot{q}}w + M_\theta^{\dot{q}}\theta + M_\phi^{\dot{q}}\phi + M_\psi^{\dot{q}}\psi + M_q^{\dot{q}}q + M_p^{\dot{q}}p + M_r^{\dot{q}}r + M_{\delta_{pit}}^{\dot{q}}\delta_{pit} + M_{\delta_{rol}}^{\dot{q}}\delta_{rol} + M_{\delta_{yaw}}^{\dot{q}}\delta_{yaw} + M_{\delta_{rot}}^{\dot{q}}\delta_{rot} + \tau_e^{\dot{q}} \quad (6)$$

where $M_u^{\dot{q}}, M_v^{\dot{q}}, M_w^{\dot{q}}, M_\theta^{\dot{q}}, M_\phi^{\dot{q}}, M_\psi^{\dot{q}}, M_q^{\dot{q}}, M_p^{\dot{q}}, M_r^{\dot{q}}, M_{\delta_{pit}}^{\dot{q}}, M_{\delta_{rol}}^{\dot{q}}, M_{\delta_{yaw}}^{\dot{q}}, M_{\delta_{rot}}^{\dot{q}} \in \Theta$; $\tau_e^{\dot{q}}$ is the corresponding element of E , which is added to represent the unknown trim error. Given the corresponding wind tunnel test data, there exists $M_v^{\dot{q}}, M_\theta^{\dot{q}}, M_\phi^{\dot{q}}, M_\psi^{\dot{q}}, M_r^{\dot{q}}, M_{\delta_{yaw}}^{\dot{q}} \approx 0$. Thus, Equation (6) can be simplified as:

$$\dot{q} = M_u^{\dot{q}}u + M_w^{\dot{q}}w + M_q^{\dot{q}}q + M_p^{\dot{q}}p + M_{\delta_{pit}}^{\dot{q}}\delta_{pit} + M_{\delta_{rol}}^{\dot{q}}\delta_{rol} + M_{\delta_{rot}}^{\dot{q}}\delta_{rot} + \tau_e^{\dot{q}} \quad (7)$$

For simplicity in the design, the transfer function of the actuator is specified by the input-output relation:

$$G_a(s) = \frac{\delta_{pit}(s)}{\delta_{piti}(s)} = \frac{1}{T_a s + 1} \quad (8)$$

It must be pointed out, however, that the proper control system for the electric servo actuator can easily be developed by means of cascade compensation networks or an actuator compensator, and many related algorithms are available for a high-performance servo control system in the literature.

Substituting Equation (8) into Equation (7) yields:

$$T_a \ddot{q} + (1 - T_a M_q^{\dot{q}}) \dot{q} - M_q^{\dot{q}} q = M_{\delta_{pit}}^{\dot{q}} \delta_{piti} + M_u^{\dot{q}} u_d + M_w^{\dot{q}} w_d + M_p^{\dot{q}} p_d + M_{\delta_{rol}}^{\dot{q}} \delta_{rol d} + M_{\delta_{rot}}^{\dot{q}} \delta_{rot d} + \tau_e^{\dot{q}} \quad (9)$$

where T_a and $M_q^{\dot{q}}$ should satisfy the following constraints:

$$1 - T_a M_q^{\dot{q}} > 0 \quad (10a)$$

$$M_q^{\dot{q}} < 0 \quad (10b)$$

which explicitly indicate that actuator dynamics can potentially destabilize the overall system of the MAV.

We now define the identification model of the system in Equation (9) as follows:

$$T_a \ddot{q}_m + a_{\dot{q}} \dot{q}_m + a_q q_m = b_{\delta_{pit}} \delta_{piti} + b_u u_d + b_w w_d + b_p p_d + b_{\delta_{rol}} \delta_{rol d} + b_{\delta_{rot}} \delta_{rot d} + b_e \quad (11)$$

where the identification parameters should satisfy the following constraints:

$$a_{\dot{q}} > 0, a_q > 0 \quad (12)$$

The error between q_m and q is expressed as:

$$e = q_m - q \quad (13)$$

Substituting Equations (9) and (11) into Equation (13) yields:

$$T_a \ddot{e} + a_{\dot{q}} \dot{e} + a_q e = -\Delta a_{\dot{q}} \dot{q} - \Delta a_q q + \Delta b_{\delta_{pit}} \delta_{pit} + \Delta b_u u_d + \Delta b_w w_d + \Delta b_p p_d + \Delta b_{\delta_{rol}} \delta_{rol} + \Delta b_{\delta_{rot}} \delta_{rot} + \Delta b_e \quad (14)$$

where:

$$\begin{cases} \Delta a_q = a_q + M_q^{\dot{q}} \\ \Delta a_{\dot{q}} = a_{\dot{q}} - 1 + T_a M_q^{\dot{q}} \\ \Delta b_u = b_u - M_u^{\dot{q}} \\ \Delta b_w = b_w - M_w^{\dot{q}} \\ \Delta b_p = b_p - M_p^{\dot{q}} \\ \Delta b_{\delta_{rol}} = b_{\delta_{rol}} - M_{\delta_{rol}}^{\dot{q}} \\ \Delta b_{\delta_{rot}} = b_{\delta_{rot}} - M_{\delta_{rot}}^{\dot{q}} \\ \Delta b_e = b_e - \tau_e^{\dot{q}} \end{cases} \quad (15)$$

However, $u_d, w_d, p_d, \delta_{rol}$ and δ_{rot} are also difficult to measure and are, therefore, not available. According to linear system theory, Equation (14) can then be approximately represented as:

$$T_a \ddot{e}_f + a_{\dot{q}} \dot{e}_f + a_q e_f = -\Delta a_{\dot{q}} \dot{q}_f - \Delta a_q q_f + \Delta b_{\delta_{pit}} \delta_{pit} + \Delta b_u u_{df} + \Delta b_w w_{df} + \Delta b_p p_{df} + \Delta b_{\delta_{rol}} \delta_{rol} + \Delta b_{\delta_{rot}} \delta_{rot} + \Delta b_e \quad (16)$$

Note that $e_f, p_{df}, q_f, u_{df}, w_{df}, \delta_{pit}, \delta_{rol}$ and δ_{rot} become easily computable with a proper $G_f(s)$, and we return to this point later.

Consider the Lyapunov function candidate:

$$V = T_a \dot{e}_f^2 + a_q e_f^2 + \Delta^T \Lambda \Delta \quad (17)$$

where $\Delta = [\Delta a_{\dot{q}}, \Delta a_q, \Delta b_{\delta_{pit}}, \Delta b_u, \Delta b_w, \Delta b_p, \Delta b_{\delta_{rol}}, \Delta b_{\delta_{rot}}, \Delta b_e]^T$, $\Lambda = \text{diag}(\lambda_{\dot{q}}, \lambda_q, \lambda_{\delta_{pit}}, \lambda_u, \lambda_w, \lambda_p, \lambda_{\delta_{rol}}, \lambda_{\delta_{rot}}, \lambda_e)$. We can therefore conclude that \dot{V} is negative definite only if:

$$\Delta^T (\mathbf{R}_f \dot{e}_f + \Lambda \dot{\mathbf{K}}) \leq 0 \quad (18)$$

where $\mathbf{R}_f = [-\dot{q}_f, -q_f, \delta_{pit}, u_{df}, w_{df}, p_{df}, \delta_{rol}, \delta_{rot}, 1]^T$ and $\mathbf{K} = [a_{\dot{q}}, a_q, b_{\delta_{pit}}, b_u, b_w, b_p, b_{\delta_{rol}}, b_{\delta_{rot}}, b_e]^T$. In fact, a similar reasoning can be made for the system given by Equation (14), and the global asymptotic convergence of the error e is guaranteed under the constraint in Equation (18). In particular, the Constraint (18) holds if the parameter regulation algorithm is represented as:

$$\dot{\mathbf{K}} = -\Gamma \mathbf{R}_f (\dot{e}_f + \varepsilon_f) \quad (19)$$

where $\Gamma = \Lambda^{-1} \stackrel{\text{def}}{=} \text{diag}(\rho_{\dot{q}}, \rho_q, \rho_{\delta_{pit}}, \rho_u, \rho_w, \rho_p, \rho_{\delta_{rol}}, \rho_{\delta_{rot}}, \rho_e)$; ε_f is optional and satisfies the constraint as follows:

$$\text{sgn}(\varepsilon_f) = \text{sgn}(T_a \ddot{e}_f + a_{\dot{q}} \dot{e}_f + a_q e_f) \quad (20)$$

The identification parameters can therefore quickly converge to the corresponding parameters of the plant in Equation (9), because ε_f is optional and can largely contribute to the convergence. To suppress the possible oscillations of identification parameters, the variation rate of \mathbf{K} is assumed to be bounded by the optional upper bound Υ :

$$\|\dot{\mathbf{K}}\|_{\infty} < \Upsilon \quad (21)$$

Remarks

i. As for the constraint given by inequality (10), on the one hand T_a should be chosen small enough such that inequality (10a) holds at any time, but on the other it is necessary beforehand to add a feedback signal like $k_{q_0}q$ to the input signal δ_{piti} without any modification of the parameter regulation strategy if inequality (10b) cannot hold in some cases, where k_{q_0} is used to guarantee the stability of the plant.

ii. The importance of the proper choice of $G_f(s)$ has been mentioned above. Here we assume that:

$$\begin{cases} G_f(s) = G_{f1}(s)G_{f2}(s) \\ G_{f1}(s) = \frac{1}{T_{f1}s + 1} \\ G_{f2}(s) = \frac{1}{T_{f2}s + 1} \end{cases} \tag{22}$$

Thus, for any variable of interest χ , we have:

$$\begin{cases} \dot{\chi}_f = \frac{1}{T_{f2}}(\chi_{f1} - \chi_f) \\ \ddot{\chi}_f = \frac{1}{T_{f1}T_{f2}}(\chi - \chi_{f1} - \chi_{f2} + \chi_f) \end{cases} \tag{23}$$

where χ_f, χ_{f1} and χ_{f2} are acted as the outputs of G_f, G_{f1} and G_{f2} in response to χ , respectively. Thus, we can conclude that the adaptive laws given by Equations (19) and (20) are computable.

iii. ε_f can be chosen as $\beta(T_a\ddot{e}_f + a_q\dot{e}_f + a_qe_f)^{2m+1}$ or $\beta\text{sgn}(T_a\ddot{e}_f + a_q\dot{e}_f + a_qe_f)$, etc., where $\beta > 0$ and $m = 0, \pm 1, \dots$. The deliberate choice of ε_f can speed up the convergence rates of identification parameters.

3.2. The Adaptive Gain Scheduling Algorithm

To realize the adaptation of the control gains of the plant and reduce the chatter in the input signal of the actuator, we employ the following control law:

$$\delta_{piti} = \frac{1}{b_{\delta_{pit}}} \left\{ b_{\delta_{pit}}^* \delta_{pitc} + (a_{\dot{q}} - a_q^*)\dot{q}_m + (a_q - a_q^*)q_m - b_u u - b_w w - b_p p - b_{\delta_{rol}} \delta_{rol} - b_{\delta_{rot}} \delta_{rot} - b_e \right\} \tag{24}$$

where $b_{\delta_{pit}}^*, a_q^*$ and $a_{\dot{q}}^*$ should be determined according to the requirements for the flying qualities and the anti-interference and anti-noise performance; δ_{pitc} denotes the attitude control signal of the pitch axis. Note that we employ $\dot{q}_m, u, w, p, \delta_{rol}, \delta_{rot}$ rather than $\dot{q}, u_d, w_d, p_d, \delta_{rol_d}, \delta_{rot_d}$ to design the rate loop, mainly because the latter with differential calculations may increase the chatter in the input signal of the actuator in the presence of measurement noises.

As the identification parameters are considered to have converged sufficiently close to the corresponding parameters of the plant, the plant can be approximately expressed as:

$$T_a\ddot{q} + a_{\dot{q}}^*\dot{q} + a_q^*q \approx b_{\delta_{pit}}^* \delta_{pitc} + \delta_e \tag{25}$$

where:

$$\delta_e = T_a (b_u \dot{u} + b_w \dot{w} + b_p \dot{p} + b_{\delta_{rol}} \dot{\delta}_{rol} + b_{\delta_{rot}} \dot{\delta}_{rot}) \tag{26}$$

As a matter of fact, changes in u, w, p, δ_{rol} and δ_{rot} occur slowly and are constrained within relatively tight bounds because the MAV is used mainly for low-speed flight missions, which means $\dot{u}, \dot{w}, \dot{p}, \dot{\delta}_{rol}$ and $\dot{\delta}_{rot}$ remain relatively small. Furthermore, T_a is also very small. Thus, we can conclude that δ_e can be negligible. Equation (25) can be further simplified to obtain:

$$T_a \ddot{q} + a_q^* \dot{q} + a_q^* q \approx b_{\delta_{pit}}^* \delta_{pitc} \tag{27}$$

The combination of online parameter estimation and the adaptive gain scheduling algorithms can accommodate parametric uncertainties and eliminate the cross coupling among all axes, thus improving the control quality of the MAV. The conventional PD control law can then guarantee the attitude control performance:

$$\delta_{pitc} = k_p e_\theta + k_d \dot{e}_\theta \tag{28}$$

where:

$$e_\theta = \theta_c - \theta \tag{29}$$

4. Numerical and Experimental Tests

The performance of the proposed strategy is demonstrated for the prototype ducted fan MAV. The predefined parameters are given as follows:

- (1) The time constants: $T_a = 0.1$ and $T_{f1} = T_{f2} = 0.02$;
- (2) The desired model parameters: $a_{\dot{q}}^* = 1.25, a_q^* = 4.2, b_{\delta_{pit}}^* = 3.0$;
- (3) The initial values of identification parameters: $a_q(0), b_u(0), b_w(0), b_p(0), b_{\delta_{rol}}(0), b_{\delta_{rot}}(0)$ and $b_e(0)$ are assumed to equal zero; $b_{\delta_{pit}}(0) = 2.2$;
- (4) The parameter estimation algorithm: $\rho_{\dot{q}}, \rho_q, \rho_{\delta_{pit}}, \rho_u, \rho_w, \rho_p, \rho_{\delta_{rol}}, \rho_{\delta_{rot}}, \rho_e = 1.0$, $\epsilon_f = 2(T_a \ddot{e}_f + a_q \dot{e}_f + a_q e_f)$, and $\Upsilon = 2.0$;
- (5) The attitude controller: $k_p = 3.0, k_d = 0.3$.

The proposed strategy is first implemented in a numerical simulation based on the data-based dynamics model. It is then applied to the MAV to evaluate the flight performance.

4.1. Numerical Simulation

For the pitch axis of the MAV, the simulation is conducted to evaluate the step response performance using the data-based dynamics model in [27]. It is illustrated from Figure 3a that the proposed strategy can achieve good dynamic performance within a short period of time even without any prior information about the behavior of the MAV. As shown in Figure 3b,c, the response of the model can match rapidly and approximately with the real response even within the first period of the square wave signal; the tracking error can remain in a bounded range for the aggressive maneuvers, which demonstrates the improved tracking accuracy in the simulation. The outputs of the roll axis caused by the coupling among axes, shown in Figure 3d,e, also remain bounded. Therefore, the proposed strategy can improve the control qualities of the MAV. Meanwhile, the parameter estimation algorithm has a good convergence property and achieves a guaranteed model reference tracking performance.

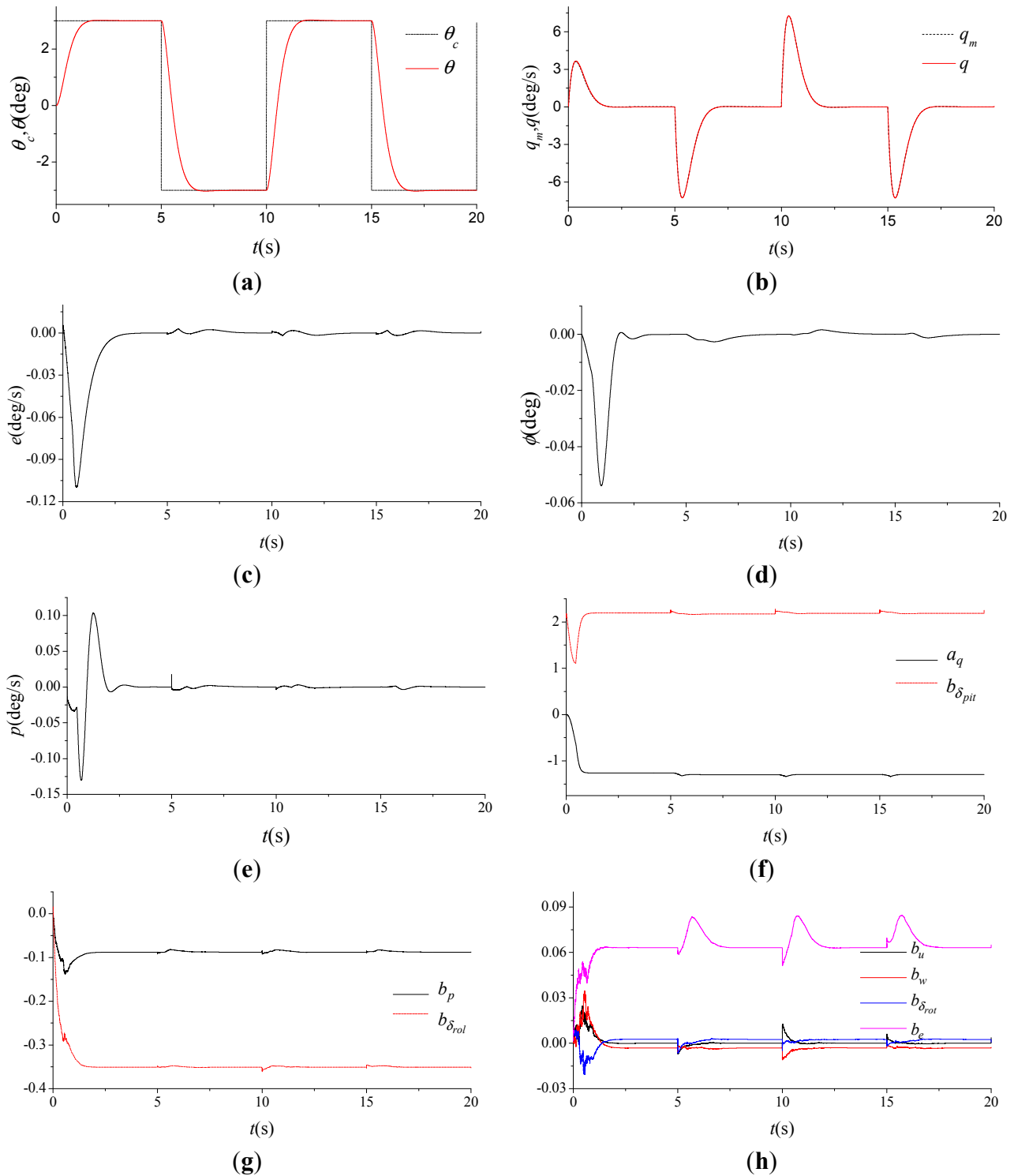


Figure 3. Numerical simulation results of the proposed strategy. (a) θ_c and θ ; (b) q_m and q ; (c) e ; (d) ϕ ; (e) p ; (f), (g) and (h) Identification parameters.

4.2. Near-hover Flight Tests

The control software system runs on a high performance DSP-based hardware platform (TI TMS320F28335) with a control period of 10 ms. The platform also provides a high precision timer, eight 16-bit pulse width modulation (PWM) channels for controlling the actuators of the MAV and several serial ports for data transmission and communication with external devices. The light-weight

sensor unit, with an update rate of 200 Hz, includes a MEMS-based Inertial Measurement Unit (IMU), a differential GPS and an Extended Kalman Filter, which can provide a smooth position, velocity and attitude solution by fusing the measurements from the IMU and GPS. As shown in Figure 4, the near-hover flight tests are subsequently conducted to compare the performance of the proposed strategy with that of the conventional controller. For a fair comparison, all flight tests begin with hover, followed by simple way-point navigation, and the flight test data of the proposed strategy are recorded for comparison after the identification parameters reach a near-steady state. The results for a period of time from these flight tests are shown in Figures 5 and 6.



Figure 4. Flight test.

The performance of the proposed strategy is first evaluated at low speeds where a square pattern is flown. The noisy tracking error, shown in Figure 5c, is within an acceptable range. The ground track view of trajectory, shown in Figure 5g, illustrates that the proposed strategy can almost eliminate the moving oscillations during the whole test process even though there exists the significant coupling between the pitch and roll axes shown in Figure 5e. We can therefore conclude that the proposed strategy can achieve a guaranteed flight performance.

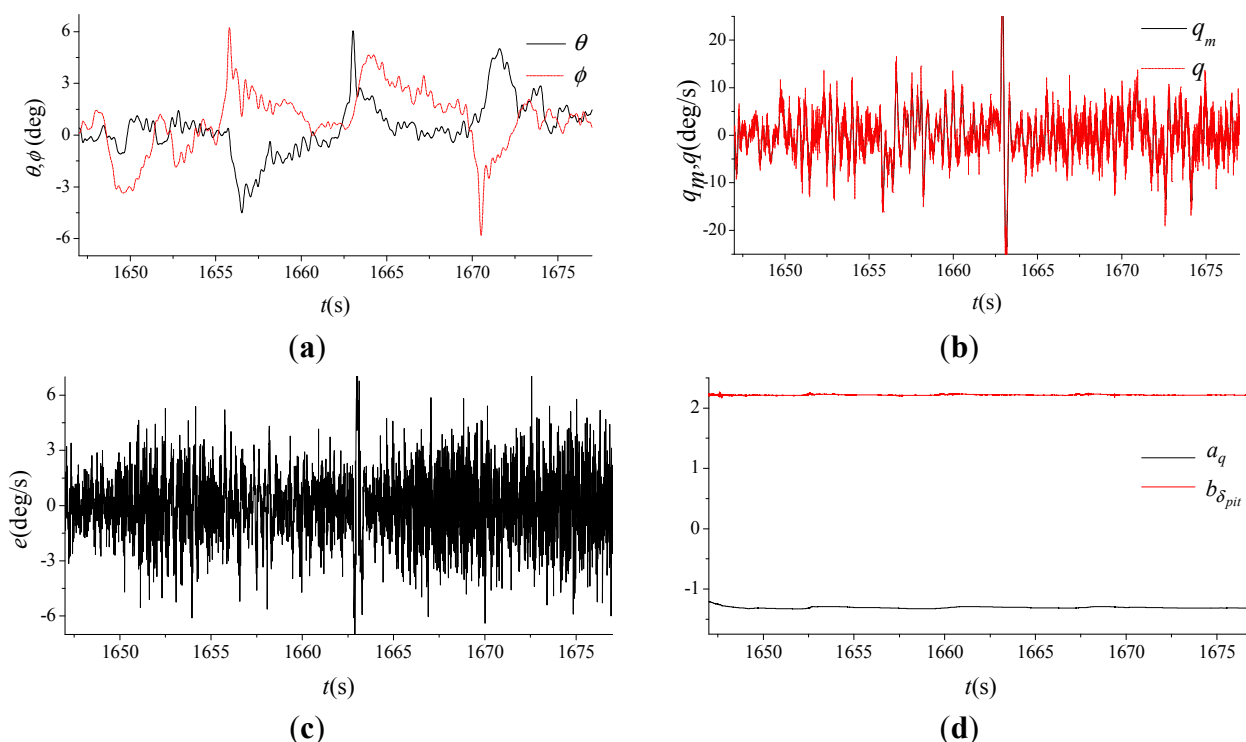


Figure 5. Cont.

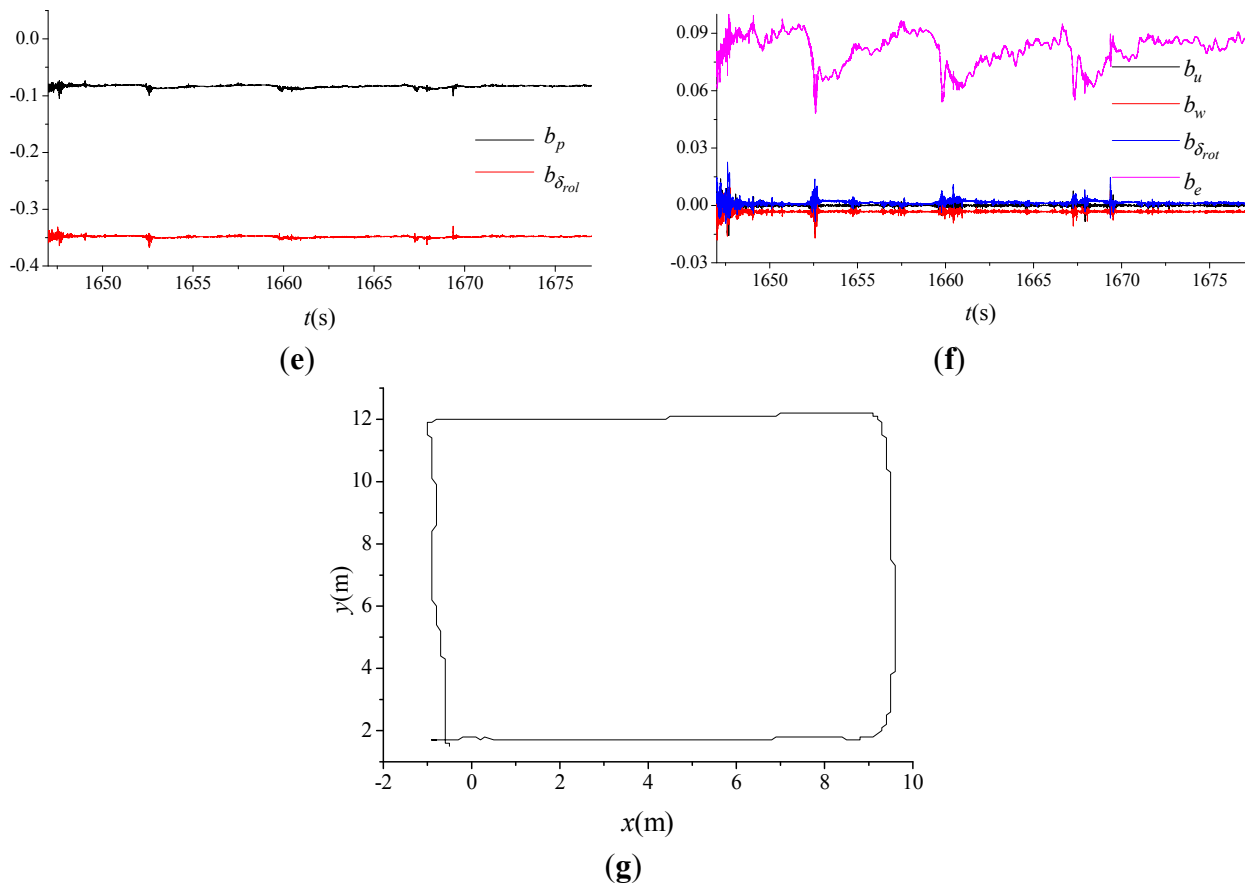


Figure 5. Test results of the proposed strategy. (a) θ and ϕ ; (b) q_m and q ; (c) e ; (d); (e) and (f) Identification parameters; (g) The ground track view of trajectory.

However, the flight test results of the conventional controller implemented through the widely used Pixhawk autopilot module, shown in Figure 6, appear to deteriorate significantly, mainly because the conventional controller cannot accommodate the unknown system parameters or eliminate the coupling among axes.

The results also show that the variations of the attitude angles and the dynamic displacements increase significantly, and the moving oscillations are quite obvious when the MAV is commanded to perform the same flight mission. The comparison of the above two flight test results have further verified the proposed strategy performs better than the conventional controller near hover.

5. Conclusions

This paper presents the near-hover adaptive attitude control strategy of the prototype ducted fan MAV with actuator dynamics and without any prior information about the behavior of the MAV. The proposed strategy consists of the online parameter estimation algorithm and the adaptive gain scheduling algorithm, with the former accommodating parametric uncertainties, and the latter approximately eliminating the coupling among axes and guaranteeing the control quality of the MAV, thus minimizing the moving oscillations. The numerical and experimental test results have illustrated that the proposed strategy significantly improves the control qualities of the MAV. Moreover, most existing control methods would require accurate models, while the proposed strategy does not.

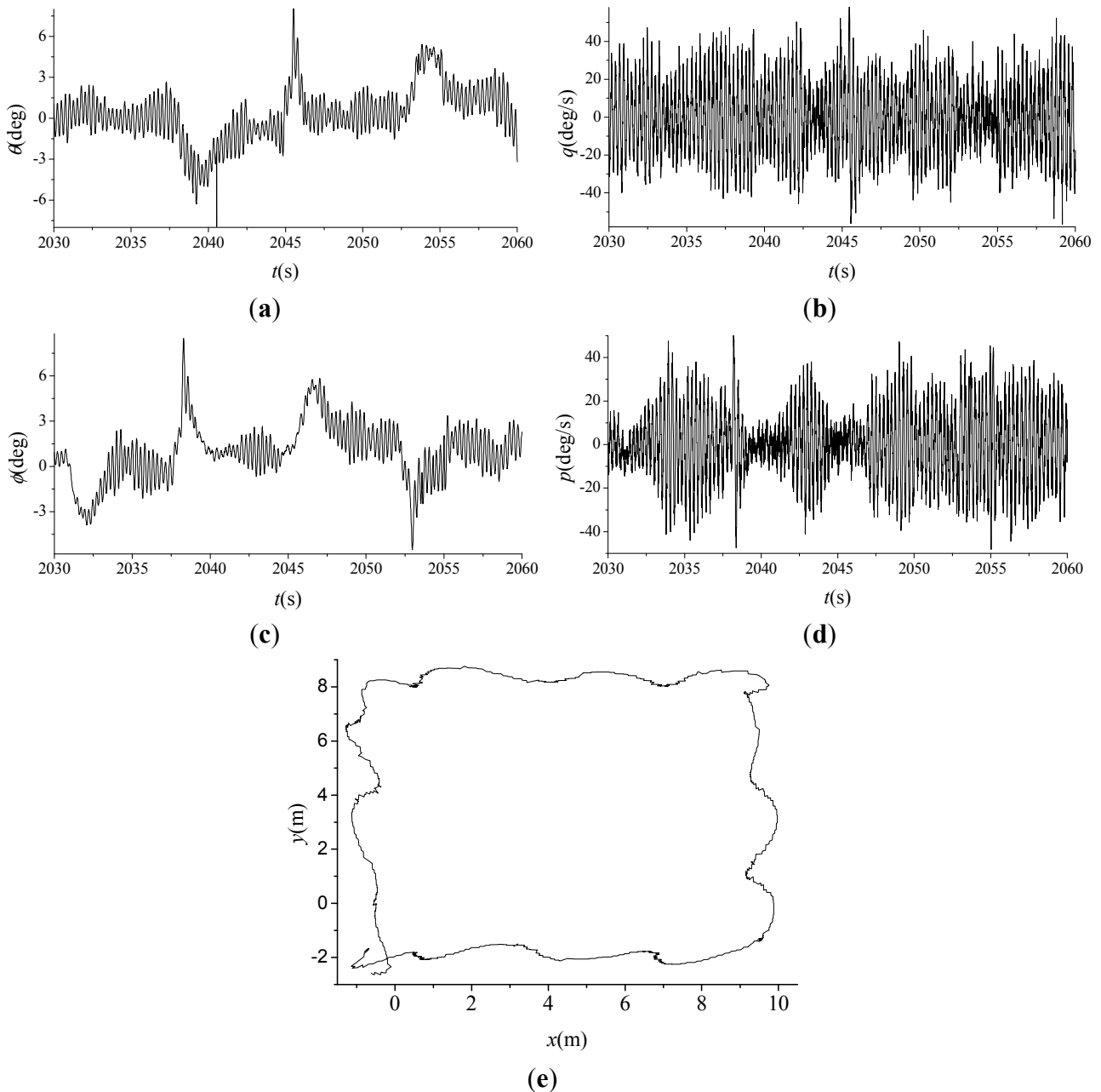


Figure 6. Test results of the conventional controller. (a) θ ; (b) q ; (c) ϕ ; (d) p ; (e) The ground track view of trajectory.

Acknowledgments

This study was supported in part by National Natural Science Foundation of China (NSFC) (Under Grant No. 61374188), Aeronautical Science Foundation of China (Under Grant No. 2013ZC52033), Natural Science Foundation of Jiangsu Province of China (Under Grant No. BK20141412), Applied Basic Research Programs of Natural Science Foundation of Jiangsu Province, China (Under Grant No. BY2015003-10).

Author Contributions

All authors discussed the contents of the manuscript. Shouzhao Sheng contributed to the research idea and the framework of this study. Chenwu Sun performed the experimental work.

Conflicts of Interest

The authors declare no conflict of interest.

Nomenclature

$a_q, a_{\dot{q}}, b_u, b_w, b_p, b_{\delta_{pit}}, b_{\delta_{rol}}, b_{\delta_{rot}}, b_e$	identification parameters
$a_q^*, a_{\dot{q}}^*, b_{\delta_{pit}}^*$	desired model parameters
A, B	system matrix and control matrix
e	tracking error
e_0	attitude tracking error
E	unknown equivalent trim error vector
f	nonlinear kinematic function
G_a	actuator transfer function
G_f, G_{f1}, G_{f2}	filter transfer functions
k_p, k_d	proportional and differential coefficients
k_{q0}	predetermined feedback gain
K	identification parameter vector
$M_u^{\dot{q}}, M_v^{\dot{q}}, M_w^{\dot{q}}, M_\theta^{\dot{q}}, M_\phi^{\dot{q}}, M_\psi^{\dot{q}}, M_q^{\dot{q}}, M_p^{\dot{q}}, M_r^{\dot{q}}, M_{\delta_{pit}}^{\dot{q}}, M_{\delta_{rol}}^{\dot{q}}, M_{\delta_{yaw}}^{\dot{q}}, M_{\delta_{rot}}^{\dot{q}}$	aerodynamic parameters
p, q, r	linearized roll, pitch and yaw rates, deg/s
$\hat{p}, \hat{q}, \hat{r}$	roll, pitch and yaw rates, deg/s
q_m	identification model output
R_f	filtered state and input vector
T_a, T_{f1}, T_{f2}	time constants of G_a, G_{f1} and G_{f2} , respectively
\tilde{U}, U	input vector and its linearized version
U_e, \tilde{U}_e	trim input vector and its estimate error
U_0	nominal trim input vector
u, v, w	linearized forward, lateral and vertical velocities, m/s
$\hat{u}, \hat{v}, \hat{w}$	forward, lateral and vertical velocities, m/s
V	Lyapunov function candidate
\hat{X}, X	state vector and its linearized version
X_0	nominal trim state vector
β	optional positive number
$\Delta a_q, \Delta a_{\dot{q}}, \Delta b_{\delta_{pit}}, \Delta b_u, \Delta b_w, \Delta b_p, \Delta b_{\delta_{rol}}, \Delta b_{\delta_{rot}}, \Delta b_e$	identification parameter errors
A	identification parameter error vector
δ_e	equivalent input disturbance

$\widehat{\delta}_l, \widehat{\delta}_r, \widehat{\delta}_f, \widehat{\delta}_b$	movements of the left, right, front and back servo motors, respectively, deg
$\delta_{pit}, \delta_{rol}, \delta_{yaw}, \delta_{rot}$	linearized manipulated input signals of pitch axis, roll axis, yaw axis and rotational speed of the ducted fan, respectively, deg
$\widehat{\delta}_{pit}, \widehat{\delta}_{rol}, \widehat{\delta}_{yaw}, \widehat{\delta}_{rot}$	manipulated input signals of pitch axis, roll axis, yaw axis and rotational speed of the ducted fan, respectively, deg
δ_{piti}	input signal of actuator
δ_{pic}	attitude control signal
Γ	A^{-1}
ε_f	optional component part of learning laws
A	optional positive definite diagonal matrix
$\lambda_{\dot{q}}, \lambda_q, \lambda_{\delta_{pit}}, \lambda_u, \lambda_w, \lambda_p, \lambda_{\delta_{rol}}, \lambda_{\delta_{rot}}, \lambda_e$	diagonal elements of A
Θ	unknown aerodynamic parameter set
X_e, \tilde{X}_e	trim state vector and its estimate error
γ	optional positive number
θ, ϕ, ψ	linearized pitch, roll and yaw angles, deg
$\widehat{\theta}, \widehat{\phi}, \widehat{\psi}$	pitch, roll and yaw angles, deg
θ_c	pitch command, deg
$\rho_{\dot{q}}, \rho_q, \rho_{\delta_{pit}}, \rho_u, \rho_w, \rho_p, \rho_{\delta_{rol}}, \rho_{\delta_{rot}}, \rho_e$	diagonal elements of Γ
$\tau_e^{\dot{q}}$	element of E
$\ \cdot \ _{\infty}$	infinite-norm
$p_d, u_d, w_d, \delta_{roid}, \delta_{roid}$	outputs of G_a^{-1} in response to $p, u, w, \delta_{rol}, \delta_{rot}$, respectively
$e_f, p_{df}, q_f, u_{df}, w_{df}, \delta_{pitf}, \delta_{roidf}, \delta_{roidf}$	outputs of G_f in response to $e, p_d, q, u_d, w_d, \delta_{piti}, \delta_{roid}, \delta_{roid}$, respectively

References

- Walsh, D.; Cycon, J.P. The Sikorsky Cypher UAV: A multi-purpose platform with demonstrated mission flexibility. In *Annual Forum Proceedings-American Helicopter Society*; American Helicopter Society: Washington, DC, USA, 1998; Volume 54, pp. 1410–1418.
- Lipera, L.; Colbourne, J.; Tischler, M.; Mansur, M.; Rotkowitz, M.; Patangui, P. The micro craft istar micro-air vehicle: Control system design and testing. In *Annual Forum Proceedings-American Helicopter Society*; AHS International: Washington, DC, USA, 2001; Volume 57, pp. 1–11.
- Pflimlin, J.M.; Soueres, P.; Hamel, T. Hovering flight stabilization in wind gusts for a ducted fan UAV. In *Proceedings of the 43rd IEEE Conference on Decision and Control (CDC'04)*, Paradise Island, Bahamas, 14–17 December 2004; pp. 3491–3496.

4. Martin, P.; Boxwell, D. Design, analysis and experiments on a 10-inch ducted rotor VTOL UAV. In *American Helicopter Society (AHS) International Specialists Meeting on Unmanned Rotorcraft: Design, Control and Testing*; American Helicopter Society: Phoenix, AZ, USA, 2005; pp. 18–20.
5. Pereira, J.; Chopra, I.; Gessow, A. Effects of shroud design variables on hover performance of a shrouded rotor for micro air vehicle applications. In *Proceedings of the AHS International Specialists' Meeting on Unmanned Rotorcraft*, Phoenix, AZ, USA, 18–20 January 2005.
6. Salluce, D.N. Comprehensive System Identification of Ducted Fan UAVs. In *Doctoral Dissertation*; California Polytechnic State University: San Luis Obispo, CA, USA, 2004.
7. Ko, A.; Ohanian, O.J.; Gelhausen, P. Ducted fan UAV modeling and simulation in preliminary design. In *Proceedings of the AIAA Modeling and Simulation Technologies Conference and Exhibit* (No. 2007–6375), Keystone, CO, USA, 20 August 2007.
8. Johnson, E.N.; Turbe, M.A. Modeling, control, and flight testing of a small ducted fan aircraft. *J. Guid. Control Dyn.* **2006**, *29*, 769–779.
9. Metni, N.; Pflimlin, J.M.; Hamel, T.; Soueres, P. Attitude and gyro bias estimation for a VTOL UAV. *Control Eng. Pract.* **2006**, *14*, 1511–1520.
10. Peddle, I.K.; Jones, T.; Treurnicht, J. Practical near hover flight control of a ducted fan (SLADe). *Control Eng. Pract.* **2009**, *17*, 48–58.
11. Sheng, S.; Mian, A.A.; Zhao, C.; Jiang, B. Autonomous take-off and landing control for a prototype unmanned helicopter. *Control Eng. Pract.* **2010**, *18*, 1053–1059.
12. Naldi, R.; Gentili, L.; Marconi, L.; Sala, A. Design and experimental validation of a nonlinear control law for a ducted-fan miniature aerial vehicle. *Control Eng. Pract.* **2010**, *18*, 747–760.
13. Pflimlin, J.M.; Soueres, P.; Hamel, T. Position control of a ducted fan VTOL UAV in crosswind. *Int. J. Control* **2007**, *80*, 666–683.
14. Pflimlin, J.M.; Binetti, P.; Soueres, P.; Hamel, T.; Trouchet, D. Modeling and attitude control analysis of a ducted-fan micro aerial vehicle. *Control Eng. Pract.* **2010**, *18*, 209–218.
15. Hess, R.A.; Ussery, T.M. Sliding mode techniques applied to the control of a micro-air vehicle. In *Proceedings of the AIAA Guidance, Navigation, and Control Conference*, Austin, TX, USA, 12 August 2003; pp. 11–14.
16. Hess, R.A.; Bakhtiari-Nejad, M. Sliding Mode Control of a Nonlinear Model of an Unmanned Aerial Vehicle. *J. Guid. Control Dyn.* **2008**, *31*, 1163–1165.
17. Spaulding, C.M.; Mansur, M.H.; Tischler, M.B.; Hess, R.A.; Franklin, J.A. Nonlinear inversion control for a ducted fan UAV. In *Proceedings of the AIAA Atmospheric Flight Mechanics Conference and Exhibit* (No. 2005–6231), San Francisco, CA, USA, 17 August 2005.
18. Chwa, D.; Choi, J.Y.; Seo, J.H. Compensation of actuator dynamics in nonlinear missile control. *IEEE Trans. Control Syst. Technol.* **2004**, *12*, 620–626.
19. Manouchehri, A.; Hajkarami, H.; Ahmadi, M.A.S. Hovering control of a ducted fan VTOL Unmanned Aerial Vehicle (UAV) based on PID control. In *Proceedings of the 2011 International Conference on Electrical and Control Engineering (ICECE)*, Yichang, China, 16–18 September 2011; pp. 5962–5965.
20. Duan, H.; Sun, C. Pendulum-like oscillation controller for micro aerial vehicle with ducted fan based on LQR and PSO. *Sci. China Technol. Sci.* **2013**, *56*, 423–429.

21. Cai, G.; Chen, B.M.; Dong, X.; Lee, T.H. Design and implementation of a robust and nonlinear flight control system for an unmanned helicopter. *Mechatronics* **2011**, *21*, 803–820.
22. Avanzini, G.; Ciniglio, U.; Matteis, G.D. Full-envelope robust control of a shrouded-fan unmanned vehicle. *J. Guid. Control Dyn.* **2006**, *29*, 435–443.
23. Aruneshwaran, R.; Suresh, S.; Wang, J.; Venugopalan, T.K. Neural adaptive flight controller for ducted-fan UAV performing nonlinear maneuver. In Proceedings of the 2013 IEEE Symposium on Computational Intelligence for Security and Defense Applications (CISDA), Singapore, 16–19 April 2013; pp. 51–56.
24. Lee, W.; Bang, H. Control of ducted fan UAV by fuzzy gain scheduler. In Proceedings of the International Conference on Control, Automation and Systems, ICCAS'07, Seoul, Korea, 17–20 October 2007; pp. 812–816.
25. Omar, Z. Intelligent Control of a ducted-fan VTOL UAV with conventional control surfaces. In *Doctoral Dissertation*; RMIT University: Melbourne, Australia, 2010.
26. Hua, M.D.; Hamel, T.; Morin, P.; Samson, C. Control of a class of thrust-propelled underactuated vehicles and application to a VTOL drone. In Proceedings of the IEEE International Conference on Robotics and Automation, 2009. ICRA'09, Kobe, Japan, 12–17 May 2009; pp. 972–978.
27. Zhang, N. Ducted fan unmanned aircraft flight dynamics analysis and control study. In *Dissertation*; Nanjing University of Aeronautics and Astronautics: Nanjing, China, 2011.

© 2015 by the authors; licensee MDPI, Basel, Switzerland. This article is an open access article distributed under the terms and conditions of the Creative Commons Attribution license (<http://creativecommons.org/licenses/by/4.0/>).